

See discussions, stats, and author profiles for this publication at: <https://www.researchgate.net/publication/245027237>

Electrochemical Aptasensor of Human Cellular Prion Based on Multiwalled Carbon Nanotubes Modified with Dendrimers: A Platform for Connecting Redox Markers and Aptamers

ARTICLE *in* ANALYTICAL CHEMISTRY · JULY 2013

Impact Factor: 5.64 · DOI: 10.1021/ac400605p · Source: PubMed

CITATIONS

24

READS

133

4 AUTHORS, INCLUDING:



Anna Miodek

Atomic Energy and Alternative Energies Com...

18 PUBLICATIONS 74 CITATIONS

[SEE PROFILE](#)



Gabriela Milagros Castillo B.

Comenius University in Bratislava

13 PUBLICATIONS 101 CITATIONS

[SEE PROFILE](#)



Hafsa Korri-Youssoufi

Université Paris-Sud 11

80 PUBLICATIONS 1,419 CITATIONS

[SEE PROFILE](#)

Electrochemical Aptasensor of Human Cellular Prion Based on Multiwalled Carbon Nanotubes Modified with Dendrimers: A Platform for Connecting Redox Markers and Aptamers

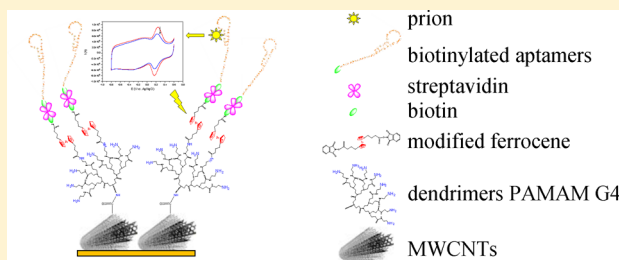
Anna Miodek,[†] Gabriela Castillo,[‡] Tibor Hianik,[‡] and Hafsa Korri-Youssoufi*,[†]

[†]UMR–CNRS 8182, ICMMO, University Paris-Sud, Bat 420 91405 Orsay France

[‡]Faculty of Mathematics, Physics and Informatics, Comenius University, Mlynska dolina F1, 84248 Bratislava, Slovakia

 Supporting Information

ABSTRACT: The present work aims to develop an electrochemical biosensor based on aptamer able to detect human cellular prions PrP^C as a model biomarker of prion disease with high sensitivity. We designed the biosensor using multiwalled carbon nanotubes (MWCNTs) modified with polyamidoamine dendrimers of fourth generation (PAMAM G4) which in turn were coupled to DNA aptamers used as bioreceptors. Electrochemical signal was detected by a ferrocenyl redox marker incorporated between the dendrimers and aptamers interlayer. MWCNTs, thanks to their nanostructure organization and electrical properties, allow the distribution of aptamers and redox markers over the electrode surface. We demonstrated that the interaction between aptamers and prion proteins leads to variation in the electrochemical signal of the ferrocenyl group. High sensitivity with a detection limit of 0.5 pM and a wide linear range of detection from 1 pM to 10 μM has been demonstrated. Detection of PrP^C in spiked blood plasma has been achieved in the same range of concentrations as for detection of PrP^C in buffer. The sensor demonstrated a recovery of minimum 85% corresponding to 1 nM PrP^C and a maximum of 127% corresponding to 1 pM PrP^C.



Prion proteins are responsible for the transmissible spongiform encephalopathies (TSEs), which is a group of fatal neurodegenerative diseases. This includes Creutzfeldt-Jakob disease in human and spongiform encephalopathy in animals.¹ The diseases are highly contagious with possible transmission from animals to humans. It is assumed that these diseases are caused by transformation of cellular prions (PrP^C) into their infectious isoform PrP^{Sc}.^{2,3} PrP^{Sc} differs from PrP^C in high content of β sheets, in resistance to protease digestion and in tendency to form large aggregates that cause formation of amyloid plaques in brain of mammals.^{4,5} Detection of prion using immunological techniques (Western blot and ELISA) is one of the most accurate methods. However, these methods are based on rather expensive antibody-enzyme conjugates, are time-consuming, and require qualified staff. Therefore the development of inexpensive, sensitive, and easy to use method for the detection of PrP^{Sc} is crucial for early diagnostics of prion diseases. Especially useful would be a point-of-care assay that can be used even by physicians, outside of specialized clinical laboratories.⁶ So far, mostly the immunodiagnostic procedure⁷ and post mortem histopathological identification of brain tissues were applied.^{8,9} However, in contrast with cerebrospinal fluid, the concentration of PrP^{Sc} in the blood is down to picomolar, which makes the measurement difficult to achieve.

Electrochemical biosensors based on DNA or RNA aptamers (aptasensors) could potentially replace existing assays for prion detection. The advantage of an electrochemical aptasensor is

the direct detection of proteins on a surface layer.¹⁰ Recent trends in development of electrochemical aptasensors are focused on application of new transducers able to improve immobilization of aptamers, sensitivity, dynamic range of detection, and allowing regenerating the sensor surface. High-sensitivity detection could be achieved in aptasensors using nanomaterials such as multiwalled carbon nanotubes (MWCNTs)¹¹ and dendrimers¹² which possess a high surface-to-volume ratio. Nanostructures such as carbon nanotubes (CNTs) have been used extensively as transducers for electrochemical biosensing analysis.¹³ MWCNTs are appropriate for covalent binding of proteins and mediators.¹⁴ These nanostructures offer a large surface to volume ratio and a very high mechanical strength. Moreover, they have unique electronic properties in enhancement of electron transport and exhibit excellent chemical and thermal stability.¹⁵ Recent studies have shown that carbon nanotubes can provide a higher surface density of immobilized biomolecules in comparison with traditional planar surfaces¹⁶ and improve significantly the electrochemical reactivity.¹⁷ In addition, lower overvoltage and high peak current were obtained in the redox response of several molecules immobilized on CNTs-modified electrodes.¹⁸

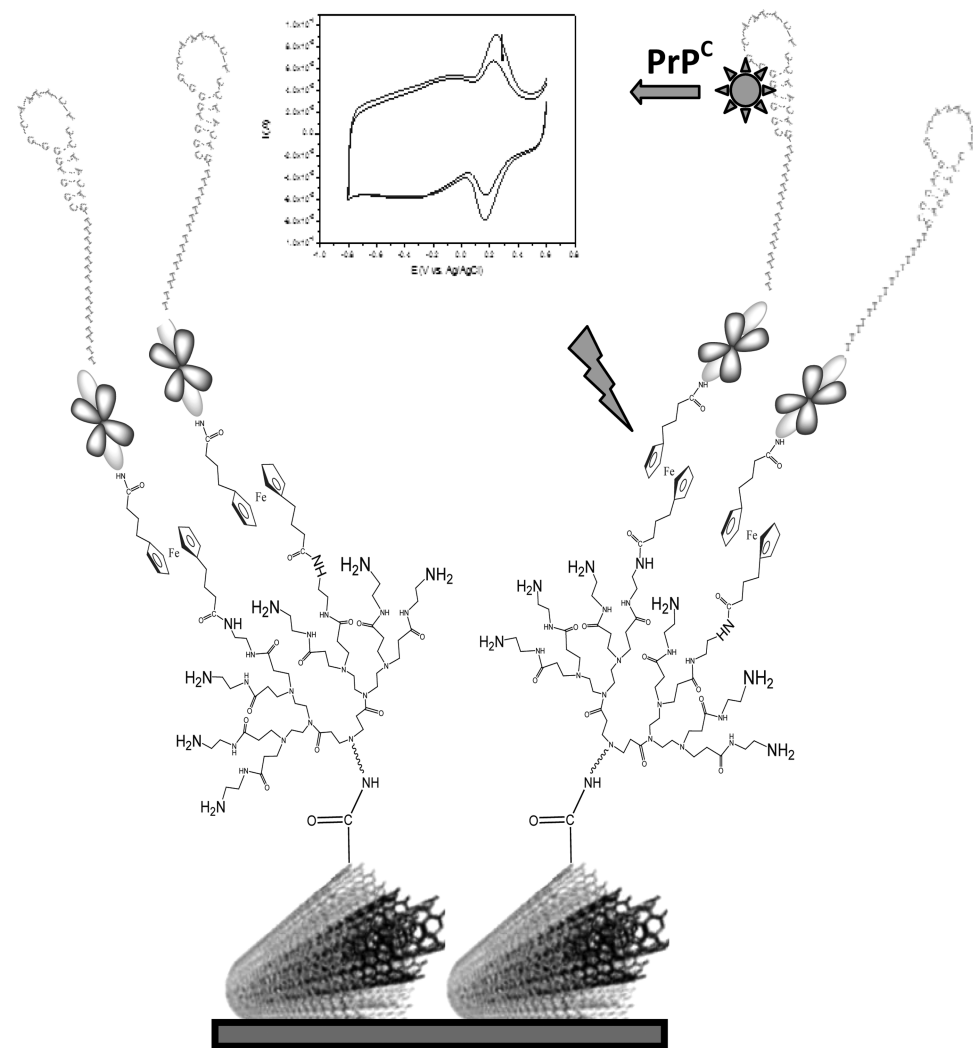
Received: February 4, 2013

Accepted: July 3, 2013

Published: July 3, 2013



Scheme 1. Schematic Representation of Biosensor Based on MWCNTs-PAMAM-Fc-Biotin-Streptavidin and Aptamer



Chemical functionalization of CNTs is an important tool for exploiting high specific surface for biosensing applications. This can be achieved by oxidation of carbon nanotubes with acidic solution for creating negatively charged carboxyl groups at the surface, which is suitable for chemical attachment of molecules bearing amine groups.¹⁹

The poly(amidoamine) dendrimers of fourth generation (PAMAM G4) have been successfully applied in the fabrication of biosensors.²⁰ They could be covalently attached to the MWCNTs through an amide link. PAMAM G4 has a globular structure with a diameter of about 4.5 nm and possesses 64 primary amine groups on the surface.²¹ The amino groups with high density in PAMAM are easily functionalized by other substances, greatly extending their applications in biosensors.²² PAMAM dendrimers in connection with MWCNTs have been successfully applied in the fabrication of electrochemical biosensors of glucose using layer-by layer methods where immobilization was performed with ionic interactions.²³

In the present paper, electrochemical biosensor for real time detection of cellular prion proteins (PrP^{C}) is described. The biosensor is based on covalent attachment of PAMAM G4 to the MWCNTs adsorbed at the surface of the gold electrode. A high number of functional groups on the surface of MWCNTs has been exploited for covalent attachment of ferrocenyl group

(Fc) as redox markers. Aptamers have been selected due to their sensitivity to prion proteins²⁴ and were immobilized on the PAMAM layer. The aptamer sequence used in this work was selected from Takemura et al.²⁵ and it was extended by a 15-mer thymine spacer in order to provide more flexibility of the aptamers after their anchoring to the supporting layer. This aptamer is part of a stem looplike structure where the GTGGGGCA sequence is involved in binding to human recombinant PrP^{C} and does not exhibit binding activity to PrP^{Sc} . This DNA aptamers bind human recombinant PrP^{C} (103-231) and exhibited a reduced affinity to the N-terminal residues (23-124) as was demonstrated previously with the surface plasmon resonance detection method.²⁶ Analytical performance of such aptasensors toward prion protein was analyzed by means of the redox signal of Fc. The result shows that MWCNTs-PAMAM-Fc can be used for determination of prion proteins at picomolar concentrations in a blood plasma sample.

EXPERIMENTAL SECTION

Reagents. The recombinant human cellular prion protein, PrP^{C} (Human PrP^{C} (103-231), molecular weight 15.1 kDa) and PrP^{C} (23-124) (molecular weight 11 kDa, used for study of nonspecific interactions) were purified at INRA Jouy-en-Josas

in France by Dr. Human Rezaei and Jasmina Vidic. The aptamers specific for PrP^C (103-231) with a dT₁₅ spacer and biotinylated on 3' phosphoryl terminus were designed based on the Takemura et al.²⁵ work and have the following nucleotide composition: (5'-CGG TGG GGC AAT TTC TCC TAC TGT dT₁₅-3'-Biotin). Aptamers were purchased from Thermo Fisher Scientific (Germany) and dissolved in TE buffer consisting of 10 mM tris(hydroxymethyl)aminomethane (Tris) and 1 mM ethylene diamine tetra-acetic acid (EDTA) at pH 7.6 in double distilled water and filtered by 0.22 μM membrane filters. Tris and EDTA were provided by Sigma-Aldrich. The synthesis of 1,1'-(phtalimidebutanoate) ferrocene Fc(NHP)₂ was described previously.²⁷ MWCNTs purity 85% (diameter ~20–25 nm and length ~1–5 μm) were purchased from Strem Chemicals (France). The polyamidoamine dendrimers of fourth generation (PAMAM G4) were provided by Sigma-Aldrich and filtered by 0.22 μM membrane filters before use.

Modification of MWCNTs. Preparation of MWCNTs modified by COOH groups (MWCNTs-COOH) and their activation by N-hydroxysuccimide (MWCNTs-COONHS) were performed by their oxidation in a mixture of acids and the reaction with coupling agent following the known procedure²⁸ (see the Supporting Information, section S-1).

Construction of Biosensor. The first step of the construction of the biosensor was the deposition on the gold surface of 5 μL of MWCNTs modified by activated ester (MWCNTs-COONHS) dissolved in DMF. After solvent evaporation, the modified MWCNTs-COONHS electrode was immersed in a solution of 70 μM (1 mg/mL) PAMAM G4 for 2 h at room temperature for enabling covalent binding between dendrimers and nanotubes. This reaction was studied by varying the time from 1 h, 2 h, 4 h and overnight. The time 2 h was found to be the optimum. The excess of nonreacted dendrimers were eliminated by washing the electrode several times with double distilled water and PBS buffer. Subsequently, the redox marker ferrocene modified by two phtalamido groups Fc(NHP)₂ was covalently attached to the PAMAM G4 by the amide link. Various experimental conditions were tested, such as concentration of ferrocene and time of reaction. Finally, this reaction was performed by immersing the electrode in a 1 mM solution of Fc(NHP)₂ in acetonitrile for 2 h at room temperature. The electrode was then washed with acetonitrile to eliminate the excess of ferrocene. The stability of the layer was studied by following the electrochemical signal of immobilized ferrocene. The deposition in these two steps, bonding of PAMAM and ferrocene on the electrode, was optimized in order to obtain a redox peak of ferrocene with current oxidation at around 100 μA. The next step was the covalent bonding of biotin hydrazide (2 mg/mL) on the surface, followed by immobilization of streptavidin dissolved in PBS solution at concentration 100 μg/mL and the subsequent immobilization of biotinylated aptamers (dissolved in TE buffer at a concentration of 2 μM) (see Scheme 1). After each step, the electrode was washed with distilled water. The modified electrode was stored in PBS solution at 4 °C until use. According to these parameters and by applying the optimum of conditions mentioned above, reproducibility was tested for more than 20 biosensors with the same response.

PrP^C Detection. Human cellular prion PrP^C (103-231) was detected in the range of concentration from 1 pM to 10 μM. All solutions were prepared in 10 mM PBS buffer pH 7.4. The 40 μL of PrP^C solution at the desired concentration has been

added as a drop on the sensor surface and incubated for 40 min at room temperature. The sensor was then washed in PBS buffer solution. The regeneration of the biosensor was performed by immersing the electrode in 100 mM HCl for 30 s, which resulted in removal of PrP^C from aptamers and destroyed the interactions between the aptamer and prion protein. The modified sensor was then rinsed by PBS solution.

Detection of the prion protein in human blood plasma was performed in the same range of concentrations (1 pM to 10 μM) like in a buffer (more details of the preparation of samples are in the Supporting Information, section S-7).

The instrumentation used is described in the Supporting Information, section S-2.

RESULTS AND DISCUSSION

Modification of MWCNTs and Covalent Binding of PAMAM G4 Dendrimers. Chemical modification of MWCNTs includes oxidation of the nanotubes by a mixture of H₂SO₄ and HNO₃ acids in the ratio 3:1 according to the procedure described above (see the Supporting Information, section S-1). As a result of oxidation, nanotubes were modified by –COOH groups. The attachment of modified MWCNTs by –COOH groups is obtained by physical adsorption of carbon nanotubes on the gold electrode. The structure of this surface has been examined by SEM imaging. As can be seen from Figure 1A, before functionalization by carboxylic groups,

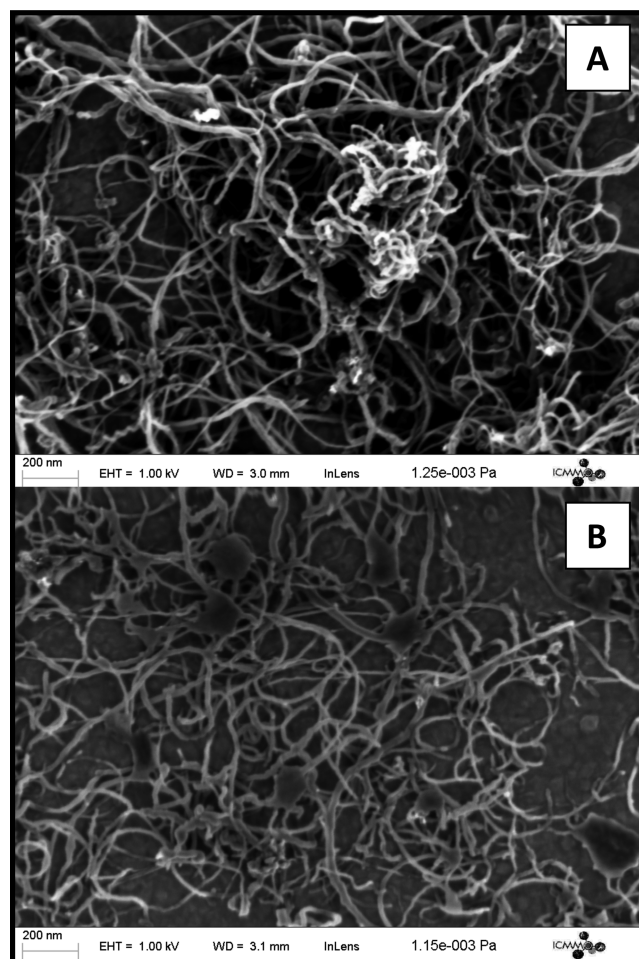


Figure 1. SEM images of gold surface covered by (A) nonmodified MWCNTs and (B) MWCNTs-PAMAM.

MWCNTs are entangled and randomly oriented on the gold surface. After the carboxylic modification obtained by oxidative treatment of MWCNTs, oxygen-containing functional groups produced in the surface of MWCNTs make the nanotubes shortened and less tangled over the gold surface where they are adsorbed by the sides (Figure 1B). This method of casting of a modified MWCNTs layer on the electrode has been generally employed for their immobilization on the gold surface.^{13,26,29} The attachment of the PAMAM dendrimers to the MWCNTs-COOH resulted in formation of globular nanoparticles on the surface of carbon nanotubes (Figure 1B). The functionalization of MWCNTs was studied by FT-IR spectroscopy (see the Supporting Information, section S-3 and Figure S-1). Modification of MWCNTs by carboxyl groups and their conjugation with PAMAM were also studied by dynamic light scattering (DLS) and laser Doppler velocimetry (LDV), which allows measuring average size (average diameter, d) of the respective nanoparticles and the ζ potential of the surface (for more details see the Supporting Information, section S-4).

Ferrocene Immobilization and Their Electrochemical Characterization. The covalent binding of ferrocenyl groups as a redox marker to the electrode surface modified by MWCNTs-PAMAM conjugates was obtained by reaction of this surface with ferrocene group modified by two active phthalimido ester groups.³⁰ This reaction allows the covalent attachment of ferrocene on MWCNTs-PAMAM by the reaction of amine groups of dendrimers with the activated ester group of ferrocene. In addition to the redox function, the ferrocene will also serve for attachment of aptamer through the biotin-streptavidin system according to the procedure described in the Experimental Section. The performance of biosensor is related to the signal response of the ferrocene where aptamers are attached and should lead to the large variation after prion interaction. For this purpose, the immobilization of ferrocene was optimized to avoid the steric hindrance due to the large size of biomolecules. The covalent attachment of ferrocene on PAMAM was subsequently performed in order to increase the ratio between aptamer attached and redox ferrocene immobilized. The characterization of covalent binding of the ferrocene group to MWCNTs-PAMAM modified electrode was analyzed by cyclic voltammetry. Figure 2A shows the CV plot of modified gold electrode by MWCNTs-PAMAM before and after covalent attachment of ferrocene. Once the covalent attachment of redox marker was performed, the appearance of characteristic, reversible redox signal of ferrocene was obtained (Figure 2A, curve b), with oxidation and reduction peaks at 0.250 and 0.180 V (vs Ag/AgCl), respectively. At relatively low scan rate, the difference between potentials of anodic and cathodic peaks was approximately 30 mV which suggests a reversible redox process. The variation of the redox signal with the scan rate was analyzed by varying the scan rate from 0.005 V/s to 0.5 V/s (see the Supporting Information, Figure S-3). The dependence of the anodic and cathodic current on the scan rate was linear. This demonstrates that the ferrocene is attached to the surface layer, and the kinetics of the redox reaction is controlled by diffusion. The relatively large current corresponding to the electron transfer from the ferrocene to the surface is observed thanks to high conductivity of carbon nanotubes. Similar behavior was obtained when redox protein such as cytochrome or hemin was immobilized on MWCNTs-PAMAM, which was attributed to the favored electron transfer.³¹ The charge exchanged during the redox process allows calculation of the surface coverage of the modified

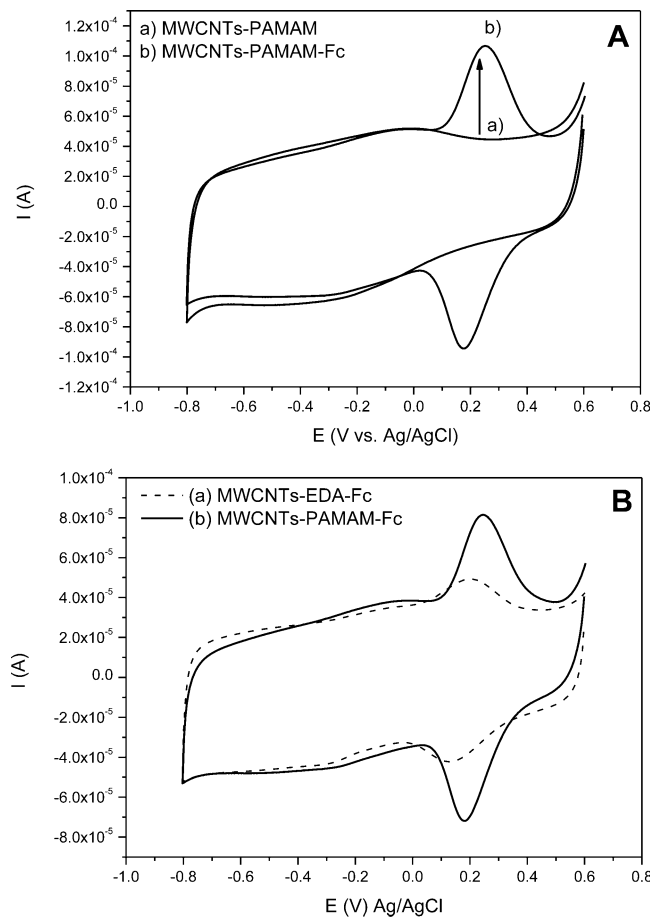


Figure 2. (A) Cyclic voltammogram of electrochemical signal of ferrocenyl group (Fc) linked to carbon nanotubes modified with dendrimers PAMAM G4 (curve b) and compared to MWCNTs before modification by Fc (curve a); (B) CV comparison of the redox signal of ferrocenyl for gold electrode covered by (a) MWCNT-EDA-Fc and (b) MWCNT-PAMAM-Fc. All CVs are recorded at the same conditions in 10 mM PBS pH 7.4 at 100 mV/s scan rate.

surface of MWCNTs-PAMAM by ferrocenyl groups following the equation

$$\Gamma = \frac{Q}{nFA}$$

where Q is the charge under the cathodic or anodic waves, n is number of electrons involved in the redox process, F is the Faraday constant, and A is the area of the electrode. We estimated that the average coverage of the surface by ferrocene was 40 nmol/cm².

PAMAM dendrimers allow increase in the number of amine groups on the surface of MWCNTs and thus binds large numbers of redox markers. In order to demonstrate the advantage of MWCNTs-PAMAM, we compared the redox properties of this system with that of the MWCNTs modified by ethylene diamine (EDA). In contrast with PAMAM, EDA allows the bonding of only one ferrocene. Figure 2B compares the redox signal of the MWCNTs-EDA-Fc layer with that of MWCNTs-PAMAM-Fc. It can be seen that the amplitude of redox peaks for MWCNTs-PAMAM-Fc (Figure 2B, solid plot) is larger in comparison with that for MWCNTs-EDA-Fc (Figure 2B, dashed plot). The charge exchanged during redox waves allows calculating an average coverage of 15 nmol/cm² of Fc group at EDA. This result clearly demonstrates higher

Table 1. Electrochemical Parameters Obtained from Electrodes of Various Modifications

biosensors	electrochemical parameters					
	$E_{1/2}$ (mV) ^a	ΔE_p (mV) ^a	Γ (10^{-9} mol/cm ²)	α	k_s (s ⁻¹)	$10^3 k_{app}$ (cm/s)
MWCNTs-EDA-Fc	112 ± 6	7 ± 2	15 ± 3	0.55	1.48 ± 0.40	7.6 ± 1.9
MWCNTs-PAMAM-Fc	189 ± 1	31 ± 0	38 ± 8	0.65	1.90 ± 0.15	8.6 ± 1.7
MWCNTs-EDA-Fc-Apt-PrP	101 ± 2	9 ± 1		0.50	1.1 ± 0.35	3.0 ± 0.3
MWCNTs-PAMAM-Fc-Apt-PrP	188 ± 2	28 ± 1		0.60	1.88 ± 0.35	2.8 ± 0.3

^aValue determined at a scan rate of 5 mV/s, and the SD was determined with three independent measurements.

coverage of Fc on the dendrimers surface in comparison with EDA containing only a single amino group. However, the signal provided by the PAMAM system is not at least 3-fold larger than that by the EDA layer as it could be expected. This low level of MWCNTs-PAMAM surface coverage could be explained by the attachment of dendrimers to MWCNTs just on their external wall-sides containing activated carboxylic functions groups and not on all of the surface of MWCNTs (see Scheme 1).

In order to analyze the kinetics of electron transfer of the ferrocene immobilized on the surface, a heterogeneous electron transfer rate (k_s) was determined following Lavoron's treatment³² based on cyclic voltammograms obtained at a higher scan rate of 0.5 V/s.

The variation in anodic potential (E_{pa}) and cathodic potential (E_{pc}) versus logarithm of the scan rate allows calculation of the coefficient of electron transfer, α , from the slope of the straight line obtained (see the Supporting Information, Figure S-3, lower inset). The slope corresponds to $2.3RT/(1 - \alpha)nF$ for the anodic potential and $-2.3RT/\alpha nF$ for the cathodic potential. The k_s value could be obtained from eq 1 following the Lavoron model.

$$\log k_s = \alpha \log(1 - \alpha) + (1 - \alpha) \log \alpha - \log \left(\frac{RT}{nF\nu} \right) - \alpha(1 - \alpha)nF \frac{\Delta E_p}{2.3RT} \quad (1)$$

The values of α and k_s obtained for ferrocene immobilized on the EDA and PAMAM surfaces are summarized in Table 1. The values of α were around 0.5, and k_s varied from 1 to 2 s⁻¹, for EDA and PAMAM surfaces, respectively. The values of k_s were of the same order of magnitude for EDA (1.48 ± 0.40) and PAMAM (1.90 ± 0.15) based surfaces. This suggests that immobilization of the ferrocenyl group at PAMAM does not disturb the kinetics of electron transfer. This agrees well with previous work demonstrating that when ferrocenyl is attached to PAMAM, the polymer chain does not disturb the electron transfer.³³

The k_s value obtained in our work has the same order of magnitude like those determined in the case of ferrocene immobilized on the gold surface through self-assembled monolayers (SAMs) or on mixed SAMs and single walled carbon nanotubes. It has been shown that k_s varied from 1 to 0.8 s⁻¹ depending on the chemical nature of the surface, onto which the ferrocene was immobilized.³⁴

Formation and Characterization of Sensing Layer. The first step in formation of the sensing layer consists of the covalent binding of biotin to the ferrocenyl group, followed by addition of streptavidin. DNA aptamers bearing biotin in their supporting part have been then attached to the streptavidin due to high affinity of biotin to the streptavidin. Further characterization of the sensing layer formation has been

performed by CV and electrochemical impedance spectroscopy methods (Figure 3). Figure 3A shows electrochemical signal of

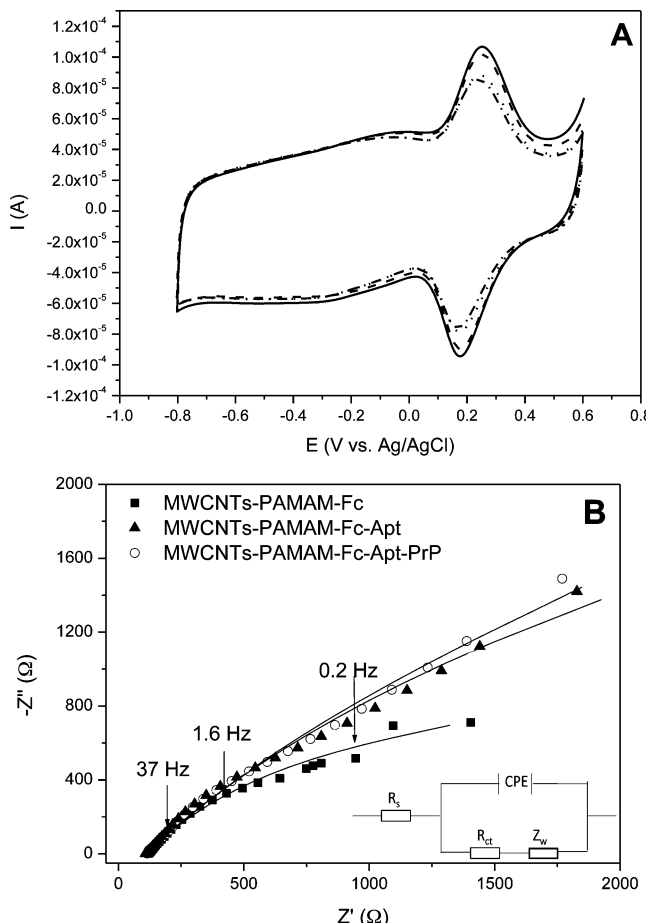


Figure 3. (A) CV data obtained after each step of biosensor formation. The CV is recorded in 10 mM PBS solution at pH 7.4 with scan rate of 100 mV s⁻¹: MWCNT-PAMAM-Fc (solid line), MWCNT-PAMAM-Fc-Biot (dashed line), MWCNT-PAMAM-Fc-Biot-Strept (dotted line), MWCNT-PAMAM-Fc-Biot-Strept-Apt (dashed dotted line). (B) Nyquist plot obtained in 5 mM/5 mM $[Fe(CN)_6]^{4-}/[Fe(CN)_6]^{3-}$ in PBS, pH 7. The measurement was obtained in the frequency range from 0.1 Hz to 100 kHz at 0.3 V vs Ag/AgCl by applying a dc potential of 10 mV. The symbols are the experimental data, and the solid are the fitted curves using the equivalent circuit showed in the inset.

ferrocenyl groups after the sensing layer's formation. A decrease in current was observed after immobilization of the aptamers. The electron transport properties through the sensing layer were studied by electrochemical impedance spectroscopy (EIS) in PBS solution containing the redox probe $[Fe(CN)_6]^{4-}/[Fe(CN)_6]^{3-}$ at pH 7. EIS measurement provides details in the

kinetics of charge transfer through the sensing layer occurring at the electrodes. Figure 3B shows the Nyquist plots obtained for the sensing layer after ferrocene immobilization and then after layer formation. The EIS data were fitted by a Randles equivalent circuit model where R_s is the electrolyte resistance, R_{ct} is the electron transfer resistance, Z_w is the Warburg impedance, while the double layer capacitance (C_{dl}) is replaced by a constant phase element (CPE). The EIS data were satisfactorily fitted by the modified equivalent circuit model shown in the inset of Figure 3B as demonstrated by the error value and allows determining the electron transfer resistance R_{ct} for each layer formation (see the Supporting Information, section S-5 and Table S-1). The R_{ct} value decreases when ferrocene is immobilized on the modified surface with PAMAM G4. This happens when ferrocene is immobilized on the surface, which permits a permeation of the redox probe and enhances the faradaic response of $[\text{Fe}(\text{CN})_6]^{4-}/[\text{Fe}(\text{CN})_6]^{3-}$ species. The formation of the sensing layer (biotin-streptavidin-aptamer) on the surface leads to an increase in the R_{ct} value. This could be related to the blocking effect of the sensing layer to the permeation of redox species to the surface of the electrode when such large molecules were immobilized on the surface.

As the experiment is performed on the formal potential of redox species $[\text{Fe}(\text{CN})_6]^{4-}/[\text{Fe}(\text{CN})_6]^{3-}$, the apparent heterogeneous electron transfer rate constant (k_{app}) could be calculated from eq 2³⁵

$$k_{app} = \frac{RT}{n^2 F^2 A R_{ct} C} \quad (2)$$

where n is the number of electrons transferred in the redox process, F is the Faraday constant, R is the gas constant, T is the temperature in Kelvin, A is the area of the electrode, and R_{ct} is the charge transfer resistance obtained from the fitted parameters of the Nyquist plot. From Table 1, it appears that k_{app} increases after ferrocene immobilization on the PAMAM surface and is in the same order of magnitude as determined previously for a surface modified with ferrocene attached to the carbon nanotube.³⁵ When the sensing layer is formed, the k_{app} decreases and this indicates that the electrochemical reaction of the redox species is slower, as electron transfer is difficult to be performed through the layer.

Electrochemical Detection of Prion. The detection of PrP^{C} (103-231) was performed in the range of concentrations from 1 pM to 10 μM . For this purpose, the biosensor was dipped into the buffer containing various concentrations of prions. The formation of the aptamer– PrP^{C} complexes was analyzed by CV. Figure 4A shows the CV signals obtained for biosensors after association of aptamers with PrP^{C} in various concentrations. It can be seen that with increasing the concentration of PrP^{C} , the peak current corresponding to the redox signal of ferrocene decreased. This decrease could be related to the low electron transfer from the ferrocenyl group to the surface due to the changes of the sensor properties caused by attachment of the prions and also to a decrease of permeability of the sensing layer after the attachment of a large molecule to the surface. In order to analyze the effect of aptamer– PrP^{C} interaction on the redox signal of ferrocene, a heterogeneous transfer constant k_s was calculated using the Laviron model for the sensor surface saturated by addition of large amount of PrP^{C} (see Ferrocene Immobilization and Their Electrochemical Characterization). The obtained k_s values are

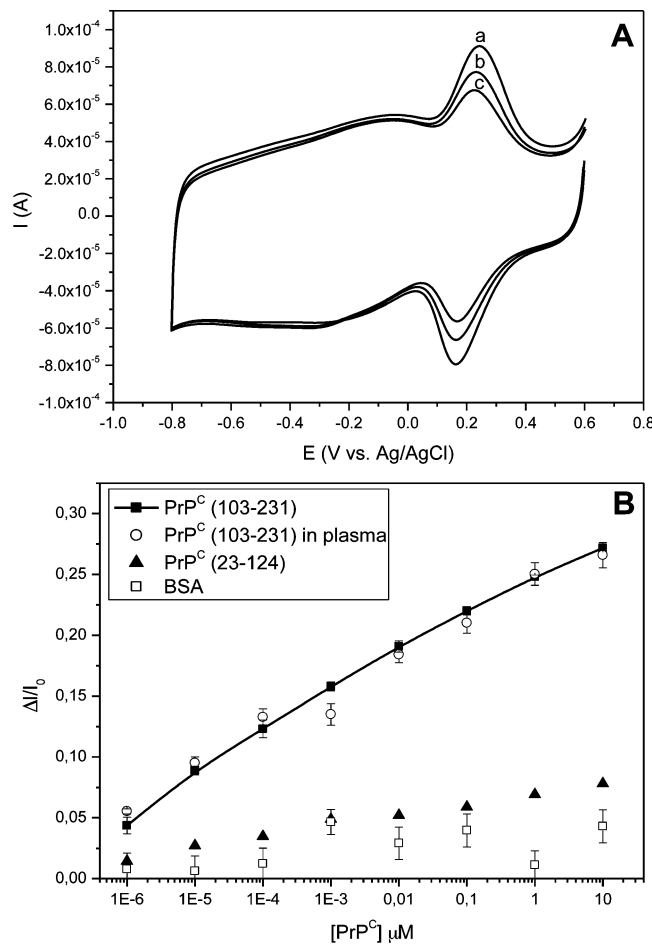


Figure 4. (A) CV of biosensors after prion protein association with aptamer at various concentrations of PrP^{C} (curve a) 0, (curve b) 1 nM, and (curve c) 10 μM . CVs were recorded in PBS solution at pH 7.4 with a scan rate 100 mV/s. (B) The plot of the relative changes of the current peak versus concentration of PrP^{C} (103-231) in plasma, PrP^{C} (23-124), and BSA. $\Delta I = (I_0 - I)$, where I_0 is the peak current prior to addition of protein and I after incubation of the sensor with certain concentrations of protein tested.

summarized in Table 1. It can be seen that k_s values decreased after addition of the prion, but this decrease is not statistically significant according to the Student's *t* test in comparison with surfaces prior to addition of prions. The rate constant, k_{app} , related to the electron transfer of redox species $[\text{Fe}(\text{CN})_6]^{4-}/[\text{Fe}(\text{CN})_6]^{3-}$ through the sensing layer after prion interaction was also calculated using the data of EIS measurements (see Figure 3B and Table 1). The k_{app} decreases after prion immobilization. This suggests that the prion interaction affects the diffusion process related to the permeability of the layer. The electron transfer between immobilized ferrocene and the nanostructured surface was not varied thanks to high conductivity of the MWCNTs. Similar behavior was observed earlier for antibody–antigen complexes at MWCNTs surface through an electroactive copper complex.²⁸

The decrease in the ferrocenyl signal during PrP^{C} detection is probably attributed to the fact that the redox marker is directly attached to the sensing layer and to the aptamers. This approach allows detecting the surface events more directly than those where the redox probe was in solution.²⁰ Detection of prion protein is based on the lower permeation of the redox markers which detect the obstruction of the electronic

communication due to the species immobilized on the sensing layer. If the sensing layer is satisfactorily assembled for allowing the signal amplification, this biosensor could be used for detection of various proteins by means of specific aptamers. Apart from size dependence of the analyte, it is also important that the aptamers binding sites maintain sufficient affinity to the target. If the binding sites are located in the surface of the protein, its detection by specific aptamers can be successfully obtained. Aptamer linkers through double strand spacers could also contribute to enhancing the aptamers mobility and their immobilization.²⁶ Additionally, changes in conformation of aptamers after binding the protein ensure a selective detection even for low molecular weight proteins.

Analysis of Analytical Performance of Biosensors.

Using the cyclic voltammograms obtained at various concentrations of PrP^C, the calibration curve presenting the plot of the relative changes of the peak current versus PrP^C concentration was prepared (Figure 4B). This calibration curve shows variation of relative changes of the current in a rather large concentration range (1 pM to 10 μM) without saturation. The detection limit was calculated based on the signal-to-noise ratio of 3 and by determining the standard deviation from three measurements. A detection limit of 0.5 pM was obtained. After aptamer immobilization, the sensors revealed similar properties toward detection of prions with a reproducibility better than 1% according to standard deviation (SD) calculated for sensor response after addition of the same concentration of PrP^C. In order to compare the response of the biosensor based on PAMAM dendrimers with that based on MWCNTs-EDA-Fc, we constructed the calibration plot also for the latter system (see the Supporting Information, Figure S-4). The MWCNTs-EDA-Fc based biosensor shows lower sensitivity to the prion protein than MWCNTs-PAMAM-Fc. EDA based biosensor also revealed the saturation of the signal at a relatively low concentration of PrP^C. Thus, replacement of PAMAM by EDA causes a reduction of the active surface and a decrease of the sensitivity of the biosensor. This proves the interest of PAMAM as a platform for receptor immobilization. Comparing the result obtained with this biosensor to those reported in the literature (Table 2), we could conclude that the electrochemical biosensors formed with MWCNTs and PAMAM connected to the ferrocenyl group as a redox marker allows measuring the prion protein with the highest sensitivity.

We also performed the studies of the stability of biosensor. After attachment of biotin on the surface, the biosensor was

stored at 4 °C for 3 nights. A small decrease of the current from 101 μA to 95 μA according to CV data was observed, which indicates a good stability of the biosensor.

The effect of nonspecific interactions of the biosensor was analyzed using the linear N-terminal part of PrP^C (23-124) which has been previously demonstrated not being complementary to the DNA aptamer used.²⁶ BSA has also been applied as a nonspecific protein. These proteins were analyzed in the same range of concentration as prion protein PrP^C (103-231) from 1 pM to 10 μM and at the same conditions.

On the basis of the changes of current corresponding to ferrocene during detection of these proteins, the calibration curves were plotted. Figure 4B shows a small response during detection of PrP^C (23-124) and BSA, which may result from nonspecific adsorption on the surface of the biosensor. This is related to the effect of BSA protein which can interact with the surface of the biosensor layer not covered by the aptamers as this protein is usually used as a blocking agent during biosensor construction. Some improvement could be realized to avoid this nonspecific interaction. Previous studies on the interaction between dendrimers with different terminal groups ($-COOH$, $-NH_2$, $-OH$) and proteins revealed that G4-dendrimers terminated by OH groups showed minimal interactions with proteins.³⁶ Hydroxyl-functionalized dendrimer was expected to be more effective in reducing nonspecific adsorption of proteins while retaining the unique structural features of the dendrimer molecule. One strategy which could be performed in the future work to reduce the effect of nonspecific interactions and simultaneously maintain the signal amplification given by dendrimers is their modification by hydroxyl groups as terminal functions.

Detection of PrP^C in Human Blood Plasma. For validating the practical application of the biosensor, 10-times diluted human blood plasma was spiked by PrP^C (103-231) in the same range of concentrations as used in PBS buffer (1 pM to 10 μM). Once prion was added, the biosensor was immersed into the spiked serum during 40 min at room temperature and rinsed in PBS buffer, and subsequently cyclic voltammograms were recorded. Three independent measurements were performed. The response of the sensor measured after incubation in plasma samples, which did not contain PrP^C, was used as a reference signal (I_0). Then the sensor response (I) was measured at certain PrP^C concentrations of spiked plasma, and the relative value $\Delta I/I_0$ has been calculated ($\Delta I = I_0 - I$). Detection of PrP^C in spiked blood plasma has been achieved in the same range of concentrations as for incubation of PrP^C in buffer. The results are presented in Figure 4B. It can be seen that the sensor response in spiked plasma agrees well with the response in PBS. The sensor demonstrated a recovery of a minimum of 85% corresponding to 1 nM PrP^C and a maximum of 127% corresponding to 1 pM PrP^C in PBS. The sensor recovery has been calculated as a ratio of the sensor response for spiked plasma and that obtained in buffer for identical prion concentrations. This ratio has been multiplied by 100 to obtain the recovery in %. The results are presented in Table S-2 in the Supporting Information. Evidently, some fraction of plasma covering the free sites of the electrode especially at the lowest prion concentrations, 1 pM, 10 pM, and 100 pM, leads to the sensor recovery values of 127%, 107%, and 108%, respectively. From spiked samples that contained 1–100 nM of prion, the sensor response was much better presenting recoveries between 85% and 96%, respectively. For the micromolar range of PrP^C concentrations (1 μM and 10

Table 2. Comparison of the Sensitivity of Various Biosensors for Detection of Cellular Prions

receptor	method	LOD	ref
aptamer	cyclic voltammetry	0.5 pM	(this work)
aptamer	SPR	4 nM	26
aptamer	EQCM	50 pM	28
aptamer	fluorescence	20 pM	37
monoclonal (mAb) and fragments (FAb) antibodies	fluorescence	nanomolar	38
monoclonal antibody, PBS buffer	fluorescence	8 nM	39
monoclonal antibodies, serum	SPR	1.4 nM	40
monoclonal antibodies, HEPES	SPR	0.57 nM	41
antibody BAR 223 or PRI 308	EQCM	20 pM, 48 pM	41

μM), the sensor recovery reached 101% and 98% of detection in plasma, respectively.

CONCLUSION

In this work we report a novel approach for the high sensitivity amperometric aptamer-based biosensor for detection of cellular prion proteins (PrP^{C}) at the picomolar concentration level. For this purpose, polyamidoamine dendrimers (PAMAM) of fourth generation (G4) were immobilized onto the multiwalled carbon nanotubes (MWCNTs). The advantage of this step consisted of providing a higher surface for immobilization of the aptamers. We approved this by comparing the sensor properties with flat construction using ethylene diamine (EDA) instead of PAMAM. The high sensitivity of amperometric detection was provided by immobilization of the ferrocene redox label between the dendrimer surface and the aptamer receptors. We have shown that the binding of prions to the surface resulted in a decrease of redox current probably due to the disturbance of electron transfer caused by conformational changes in the surface layer.

The sensor was validated in real samples of spiked human blood plasma. The results of validation approved the possibility of application of the developed platform for practical detection of PrP^{C} . High sensitivity detection of PrP^{C} by the developed aptamer based biosensor is highly promising also for the application of the reported approach for determination of pathological prions (PrP^{Sc}). The approach proposed in this work can be applied for detection of other proteins using corresponding specific aptamers.

ASSOCIATED CONTENT

Supporting Information

Additional information as noted in text. This material is available free of charge via the Internet at <http://pubs.acs.org>.

AUTHOR INFORMATION

Corresponding Author

*Phone: +33-1-69157440. Fax: +33-1-69157281. E-mail: hafsa.korri-youssoufi@u-psud.fr.

Notes

The authors declare no competing financial interest.

ACKNOWLEDGMENTS

This work was supported by French Government partenariats Hubert Curien (PHC) project Stefanie No. 23129TE, and the Slovak Research and Development Agency (Contracts APVV-0410-10 and SK-FR-0025-09), by the Slovak Academy of Sciences under the project mnt-era.net (Proposal No. 2009-50) and VEGA (Project No. 1/0785/12) by Ministry of Education and Research for fellowship to A. Miodek. We are grateful to Dr. Human Rezaei and Dr. Jasmina Vidic from the VIM group of INRA France for the generous gift of PrP^{C} proteins.

REFERENCES

- (1) Collinge, J. *Annu. Rev. Neurosci.* **2001**, *24*, 519–550.
- (2) Masters, C. L.; Gajdusek, D. C.; Gibbs, C. J. *Brain* **1981**, *104*, 559–588.
- (3) Prusiner, S. B. *Science* **1991**, *252*, 1515–1522.
- (4) Pan, K. M.; Baldwin, M.; Nguyen, J.; Gasset, M. D.; Serban, A.; Groth, D.; Mehlhorn, I.; Huang, Z.; Fletterick, J.; Cohen, F. E.; Prusiner, S. B. *Proc. Natl. Acad. Sci. U.S.A.* **1993**, *90*, 10962–10966.
- (5) Prusiner, S. B.; Scott, M. R.; DeArmond, S. J.; Cohen, F. E. *Cell* **1998**, *93*, 337–348.
- (6) Fournier-Wirth, C.; Jaffrezic-Renault, N.; Coste, J. *Transfusion* **2010**, *50*, 2032–2045.
- (7) Safar, J. G.; Geschwind, M. D.; Deering, C.; Didorenko, S.; Sattavat, M.; Sanchez, H.; Serban, A.; Vey, M.; Baron, H.; Giles, K.; Miller, B. L.; Dearmond, S. J.; Prusiner, S. B. *Proc. Natl. Acad. Sci. U.S.A.* **2005**, *102*, 3501–3506.
- (8) Kuczus, T.; Koch, R.; Keyvani, K.; Karch, H.; Grassi, J.; Groschup, M. H. *Eur. J. Neurosci.* **2007**, *25*, 2649–2655.
- (9) Kawatake, S.; Nishimura, Y.; Sakaguchi, S.; Iwaki, T.; Doh-ura, K. *Biol. Pharm. Bull.* **2006**, *29*, 927–932.
- (10) Iliuk, A. B.; Hu, L.; Tao, W. A. *Anal. Chem.* **2011**, *83*, 4440–4452.
- (11) Rohrbach, F.; Karadeniz, H.; Erdem, A.; Famulok, M.; Mayer, G. *Anal. Biochem.* **2012**, *421*, 454–459.
- (12) Zhang, Z.; Yang, W.; Wang, J.; Yang, C.; Yang, F.; Yang, X. *Talanta* **2009**, *78*, 1240–1245.
- (13) Rivas, G. A.; Rubianes, M. D.; Rodriguez, M. C.; Ferreyra, N. F.; Luque, G. L.; Pedano, M. L.; Misoria, S. A.; Parrado, C. *Talanta* **2007**, *74*, 291–307.
- (14) Wang, J.; Lin, Y. *Trends Anal. Chem.* **2008**, *27*, 619–626.
- (15) Ajayan, P. M. *Chem. Rev.* **1999**, *99*, 1787–1800.
- (16) Wang, J.; Kawde, A.; Mustafa, M. *Analyst* **2003**, *128*, 912–916.
- (17) Musameh, M.; Wang, J.; Merkoci, A.; Lin, Y. *Electrochim. Commun.* **2002**, *4*, 743–746.
- (18) Carrara, S.; Shumyantseva, V. V.; Archakov, A. I.; Samor, B. *Biosens. Bioelectron.* **2008**, *24*, 148–150.
- (19) Katz, E.; Willner, I. *Chem. Phys. Chem.* **2004**, *5*, 1085–1104.
- (20) Zhu, N.; Gao, H.; Xu, Q.; Lin, Y.; Su, L.; Mao, L. *Biosens. Bioelectron.* **2010**, *25*, 1498–1503.
- (21) Tsukruk, V. V.; Rinderspacher, F.; Bliznyuk, V. N. *Langmuir* **1997**, *13*, 2171–2176.
- (22) Wei-Jie, S.; Shi-Yun, A.; Jin-Huan, L.; Lu-Sheng, Z. *Chin. J. Anal. Chem.* **2008**, *36*, 335–338.
- (23) Zeng, Y. L.; Huang, Y. F.; Jiang, J. H.; Zhang, X. B.; Tang, C. R.; Shen, G. L.; Yu, R. Q. *Electrochim. Commun.* **2007**, *9*, 185–190.
- (24) Bibby, D. F.; Gill, A. C.; Kirby, L.; Farquhar, C. F.; Bruce, M. E.; Garson, J. A. *J. Virol. Methods* **2008**, *151*, 107–115.
- (25) Takemura, K.; Wang, P.; Vorberg, I.; Surewicz, W.; Priola, S. A.; Kanthasamy, A.; Pottathil, R.; Chen, S. G.; Sreevatsan, S. *Exp. Biol. Med.* **2006**, *231*, 204–214.
- (26) Miodek, A.; Poturnayová, A.; Šnejdárková, M.; Hianik, T.; Korri-Youssoufi, H. *Anal. Bioanal. Chem.* **2013**, *405*, 2505–2514.
- (27) Le, H. Q. A.; Chebil, S.; Makrouf, B.; Sauriat-Dorizon, H.; Mandrand, B.; Korri-Youssoufi, H. *Talanta* **2010**, *81*, 1250–1257.
- (28) Chebil, S.; Macauley, N.; Hianik, T.; Korri-Youssoufi, H. *Electroanalysis* **2013**, *25*, 636–643.
- (29) Hianik, T.; Porfireva, A.; Grman, I.; Evtugyn, G. *Prot. Pept. Lett.* **2009**, *16*, 363–367.
- (30) Korri-Youssoufi, H.; Makrouf, B. *Synth. Met.* **2001**, *119*, 265–266.
- (31) Chen, Q.; Ai, S.; Zhu, X.; Yin, H.; Ma, Q.; Qiu, Y. *Biosens. Bioelectron.* **2009**, *24*, 2991–2996.
- (32) Laviron, E. *J. Electroanal. Chem.* **1979**, *101*, 19–28.
- (33) Astruc, D.; Ornelas, C.; Ruiz, J. *Acc. Chem. Res.* **2008**, *41*, 841–856.
- (34) Nkosi, D.; Pillay, J.; Ozoemena, K. I.; Nouneh, K.; Oyamac, M. *Phys. Chem. Chem. Phys.* **2010**, *12*, 604–613.
- (35) Janek, R. P.; Fawcett, W. R.; Ulman, A. *Langmuir* **1998**, *14*, 3011–3018.
- (36) Han, H. J.; Kannan, R. M.; Wang, S.; Mao, G.; Kusanovic, J. P.; Romero, R. *Adv. Funct. Mater.* **2009**, *19*, 1–13.
- (37) Xiao, S. J.; Hu, P. P.; Li, Y. F.; Huang, C. Z.; Huang, T.; Xiao, G. F. *Talanta* **2009**, *79*, 1283–1286.
- (38) Henry, J.; Anand, A.; Chowdhury, M.; Coté, G.; Moreira, R.; Good, T. *Anal. Biochem.* **2004**, *334*, 1–8.
- (39) Anand, A.; Moreira, R.; Henry, J.; Chowdhury, M.; Coté, G.; Good, T. *LWT-Food Sci. Technol.* **2005**, *38*, 849–858.
- (40) Cuccioloni, M.; Amici, M.; Eleuteri, A. M.; Biagetti, M.; Barocci, S.; Angeletti, M. *Proteins: Struct. Funct. Bioinform.* **2005**, *58*, 728–734.

(41) Wan, J. Y.; Wang, X.; Li, J. P.; Liu, W. S.; Xu, M.; Liu, L. N.; Xu, J.; Wang, H. Y.; Gao, H. W. *Arch. Virol.* **2009**, *154*, 1901–1908.